Adjoint-based sensitivity of a thermo-acoustic system

Jiasen Wei[1], Jan Oscar Pralits[2], and Alessandro Bottaro[3]
University of Genoa, Department of Civil, Chemical and Environmental Engineering (DICCA)
via Montallegro 1, 16145, Genoa, Italy

ABSTRACT

Clean combustion, such as hydrogen combustion for the reduction of NOx emissions, is prone to thermo-acoustic instabilities which may cause structural vibrations and equipment failures. In the present work, an adjoint-based sensitivity analysis is applied to a low-order thermo-acoustic model. A structural sensitivity analysis is conducted first to evaluate the effects of a generic feedback mechanism on eigenvalues of concern. It is found that the most stabilizing feedback mechanism is the addition of mass, in a quantity which is proportional to the pressure perturbation right downstream of the flame. Sensitivity of the eigenvalues to base flow modifications is also assessed. Such analyses provide gradient information for optimization techniques to mitigate or cancel such instabilities with quick and low-cost calculations.

1. INTRODUCTION

The problem of thermo-acoustic (TA) instabilities arose with the invention of premixed combustors, designed to reduce pollution and exhaust gases. However, such systems are susceptible to destructive coupling between unsteady heat release and acoustic pressure oscillations. A wide variety of combustion systems, from domestic burners to rocket engines, suffers of such TA instabilities, which may cause structural vibrations and equipment failures [1]. TA behavior is sensitive to various parameters such as operating point, fuel composition, geometrical features, etc. Multiple research areas such as fluid mechanics, heat transfer, and acoustic wave propagation are used to model TA systems. Therefore, the phenomenon is difficult to predict and the engineering approach to eliminate it is typically expensive.

The adjoint-based approach is a powerful tool for tackling stability, receptivity, and sensitivity problems in fluid dynamics. Comparing with the traditional finite-difference approach, the adjoint method is more cost-friendly and effective in the analysis of a system which depends on many parameters. Giannetti and Luchini [2] conducted structural sensitivity of the flow around a cylinder and identified how to optimally position a small control cylinder to suppress the von Kaŕmań vortex street. Marquet et al. [3] investigated the sensitivity of eigenvalue to base-flow modifications and to a steady force. The former analysis identified the regions where base flow can affect the onset of instability. The latter analysis gave predictions of possible passive control methods to suppress the

[1]jiasen.wei@edu.unige.it

[2]jan.pralits@unige.it

[3]alessandro.bottaro@unige.it

shedding. Adjoint sensitivity analysis has also been used in shape optimization of TA systems such as the Rijke tube, swirl combustors [4], and low-order models [5]. The structural sensitivity and base-state sensitivity analyses have been applied to TA systems such as the Rijke tube [6] and wave-based low-order models [7].

The main aim of this paper is to apply the adjoint sensitivity approach to the premixed combustor model described by Dowling and Stow [8], using a low-order, lumped modelling approach. The paper consists of three parts: in section 2, we apply the low-order modelling approach to the one-dimensional TA system and solve the eigenvalue problem to predict resonant modes. The predictions obtained are validated with results from the literature. In section 3, the adjoint equations are derived from the governing base flow and perturbation equations. The adjoint eigenproblem is solved with the same numerical strategy as the direct problem. In section 4, structural and base-state sensitivities are computed, with a focus on the most unstable eigenmode. Section 5 presents the main conclusions of the work.

2. THE ONE-DIMENSIONAL PREMIXED COMBUSTOR MODEL

2.1. General Description

The system examined in this work is a one-dimensional TA model from Dowling and Stow [8]. As shown in Fig. 1, the model consists of a plenum, a premix duct and a combustion chamber. The dimensions of the model are given in Table 1. The system has a chocked inlet and an open outlet.

The flame is consider as a thin flame sheet at the intersection between the premixer and the combustion chamber. The chemical reactions are considered as instantaneous; therefore, the flame model is introduced as a jump conditions instead of as a source term in the governing equations. In each duct, the flow variables are decomposed into base flow plus perturbation, viz. $p = \bar{p} + p'$, $u = \bar{u} + u'$, $\rho = \bar{\rho} + \rho'$. The governing equations for the base flow and the perturbations are Eqs. (1) and (2), respectively, with $\gamma = C_p/C_v$ the specific heat ratio:

$$\bar{\rho}\frac{\mathrm{d}\bar{u}}{\mathrm{d}x} + \bar{u}\frac{\mathrm{d}\bar{\rho}}{\mathrm{d}x} = 0, \tag{1a}$$

$$\bar{\rho}\bar{u}\frac{\mathrm{d}\bar{u}}{\mathrm{d}x} + \frac{\mathrm{d}\bar{p}}{\mathrm{d}x} = 0, \tag{1b}$$

$$\bar{u}\frac{\mathrm{d}\bar{p}}{\mathrm{d}x} + \gamma\bar{p}\frac{\mathrm{d}\bar{u}}{\mathrm{d}x} = 0. \tag{1c}$$

$$\frac{\partial\rho'}{\partial t} + \bar{u}\frac{\partial\rho'}{\partial x} + \bar{\rho}\frac{\partial u'}{\partial x} = 0, \tag{2a}$$

$$\bar{\rho}\frac{\partial u'}{\partial t} + \bar{\rho}\bar{u}\frac{\partial u'}{\partial x} + \frac{\partial p'}{\partial x} = 0, \tag{2b}$$

$$\frac{\partial p'}{\partial t} + \bar{u}\frac{\partial p'}{\partial x} + \gamma\bar{p}\frac{\partial u'}{\partial x} = 0. \tag{2c}$$

2.2. The TALOM approach

The system is solved as an eigenvalue problem in the complex domain using an approach denominated TALOM (Thermo-Acoustic Low-Order Modelling). This is a lumped approach which expresses the system through a set of suitable equations deduced from boundary and jump conditions.

First, the base flow is computed. We consider the mean flow parameters to be uniform throughout each of the three ducts. Therefore, in the combustion chamber section, the mean flow temperature is the same as the flame temperature T_f. The unknowns for the mean flow problem are: the mean

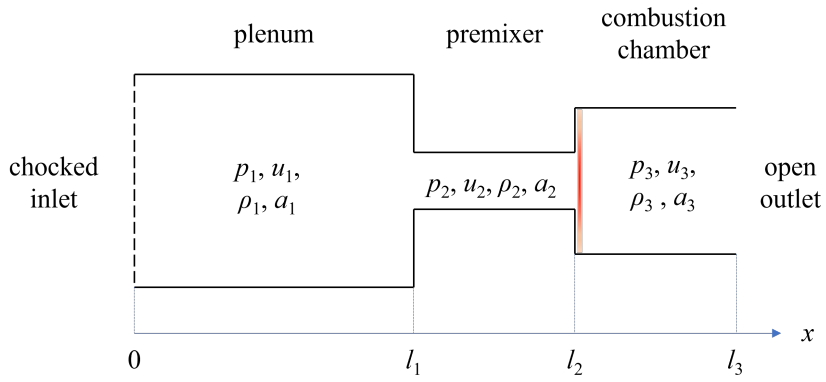

Figure 1: Sketch of the three-duct combustion model.

Table 1: Geometrical parameters of the premixed combustor model.

Description	**Symbol**	**Value**
Plenum cross-sectional area	a_1	0.0129 m^2
Plenum length	l_1	1.7 m
Premixer cross-sectional area	a_2	0.00142 m^2
Premixer length	l_2	0.0345 m
Combustion chamber cross-sectional area	a_3	0.00385 m^2
Combustion chamber length	l_3	1.0 m

heat release rate $\bar{Q}$, plus $\bar{\rho}$, $\bar{u}$, $\bar{p}$, $\bar{T}$ in each duct. To close the problem, a perfect gas state equation, $\bar{p} = \bar{\rho} R_g \bar{T}$, is applied in each duct, with R_g the perfect gas constant. The mass, momentum, and energy conservation conditions are applied at each intersection. For a sectional area increase a Borda-like equation is applied, while for a sectional area decrease the isentropic condition is imposed. The input parameters for the mean flow calculation are:

$$\bar{m}_1 = 0.05 \text{ kg/s}, \quad \bar{T}_1 = 300 \text{ K}, \quad \bar{p}_3 = 101000 \text{ Pa}, \quad \bar{T}_3 = T_f = 2000 \text{ K}. \tag{3}$$

The perturbation equations are solved in a similar manner after converting the variables in the frequency domain:

$$p'(x,t) = \hat{p}(x)e^{i\omega t}, \quad u'(x,t) = \hat{u}(x)e^{i\omega t}, \quad \rho'(x,t) = \hat{\rho}(x)e^{i\omega t}, \tag{4}$$

where $\omega = \omega_r + i\omega_i$ is the complex frequency with the real part (ω_r) representing the angular frequency of the oscillation and the negative imaginary part ($-\omega_i$) representing the growth rate. Furthermore, any disturbance can be decomposed as the sum of acoustic, entropy, and vorticity disturbances [9], with the three contributions independent of one another. For the one-dimensional case, the vorticity disturbance is not considered. Consequently, the perturbations are decoupled as:

$$\hat{p}(x) = A_+ e^{ik_+ x} + A_- e^{ik_- x}, \quad \hat{\rho}(x) = \frac{1}{\bar{c}^2} A_+ e^{ik_+ x} + \frac{1}{\bar{c}^2} A_- e^{ik_- x} - \frac{1}{\bar{c}^2} A_e e^{ik_0 x}, \quad \hat{u}(x) = -\frac{k_+}{\bar{\rho}\alpha_+} A_+ e^{ik_+ x} - \frac{k_-}{\bar{\rho}\alpha_-} A_- e^{ik_- x}, \tag{5}$$

where A_+ and A_- are the amplitudes of forward- and backward-travelling acoustic waves, respectively, A_e is the amplitude of the entropy wave and $\bar{c} = \sqrt{(\partial p/\partial \rho)_s}$ is the speed of sound. The dispersion relations are $k_\pm = \dfrac{\bar{M}\omega \mp |\omega|}{\bar{c}(1-\bar{M}^2)}$, $k_0 = -\dfrac{\omega}{\bar{u}}$, and $\alpha_\pm = \omega + \bar{u}k_\pm$, with $\bar{M} = \bar{u}/\bar{c}$ the Mach number.

The first-order linearized jump conditions at the duct intersections are given next. At the position $x = l_1$, they are:

$$a_1\left(\bar{\rho}_1\hat{u}_1 + \hat{\rho}_1\bar{u}_1\right) = a_2\left(\bar{\rho}_2\hat{u}_2 + \hat{\rho}_2\bar{u}_2\right), \quad \gamma\frac{\hat{\rho}_1}{\bar{\rho}_1} - \frac{\hat{p}_1}{\bar{p}_1} = \gamma\frac{\hat{\rho}_2}{\bar{\rho}_2} - \frac{\hat{p}_2}{\bar{p}_2}, \quad c_p\hat{T}_1 + \bar{u}_1\hat{u}_1 = c_p\hat{T}_2 + \bar{u}_2\hat{u}_2. \tag{6}$$

At $x = l_2$:

$$a_2\left(\bar{\rho}_2\hat{u}_2 + \hat{\rho}_2\bar{u}_2\right) = a_3\left(\bar{\rho}_3\hat{u}_3 + \hat{\rho}_3\bar{u}_3\right), \tag{7a}$$

$$a_2\hat{\rho}_2\bar{u}_2^2 + 2a_2\bar{\rho}_2\bar{u}_2\hat{u}_2 = a_3\left(\hat{p}_3 - \hat{p}_2\right) + a_3\hat{\rho}_3\bar{u}_3^2 + 2a_3\bar{\rho}_3\bar{u}_3\hat{u}_3, \tag{7b}$$

$$a_2\left(\bar{\rho}_2\bar{u}_2\hat{H}_2 + \bar{\rho}_2\hat{u}_2\bar{H}_2 + \hat{\rho}_2\bar{u}_2\bar{H}_2\right) = a_3\left(\bar{\rho}_3\bar{u}_3\hat{H}_3 + \bar{\rho}_3\bar{H}_3\hat{u}_3 + \bar{u}_3\bar{H}_3\hat{\rho}_3 - \hat{Q}\right), \tag{7c}$$

with the unsteady heat release rate $\hat{Q}$ defined by,

$$\hat{Q} = -\kappa\bar{Q}\frac{\hat{m}_2}{\bar{m}_2}e^{-i\omega\tau}. \tag{8}$$

The parameter κ is used to switch on or off the heat release term; $H = \frac{1}{2}u^2 + C_pT$ is the specific enthalpy. The boundary conditions of the choked inlet ($x = 0$) and open-pressure outlet ($x = l_3$) are:

$$\frac{\hat{\rho}_1(0)}{\bar{\rho}_1} + \frac{\hat{u}_1(0)}{\bar{u}_1} = 0, \quad \hat{p}_1(0) = \bar{c}_1^2\hat{\rho}_1(0), \quad \hat{p}_3(l_3) = 0. \tag{9}$$

Note that, to close the problem, the isentropic condition, Eq. (9)-middle, at $x = 0$ has been introduced. The governing equations of the system are written in matrix form, $\mathcal{A}\mathbf{q} = 0$, where $\mathbf{q}$ is the vector consisting of the decoupled independent amplitudes of acoustic and entropy waves (A_+, A_-, A_e) in each duct and $\mathcal{A}$ is the coefficient matrix. This eigenvalue problem is solved by the inverse iteration algorithm [2]. The mode shapes of the state variables are then reconstructed by the use of Eq. (5).

The spectrum of resonant modes is shown in Fig. 2 and is compared with Dowling and Stow's result. The spectrum captures well the frequencies of the dominant modes. Although the growth rate values do not coincide for all modes, the shapes of the perturbations agree well. The asymptotic behavior of the system is dominated by the least stable eigenmode, that of largest growth rate.

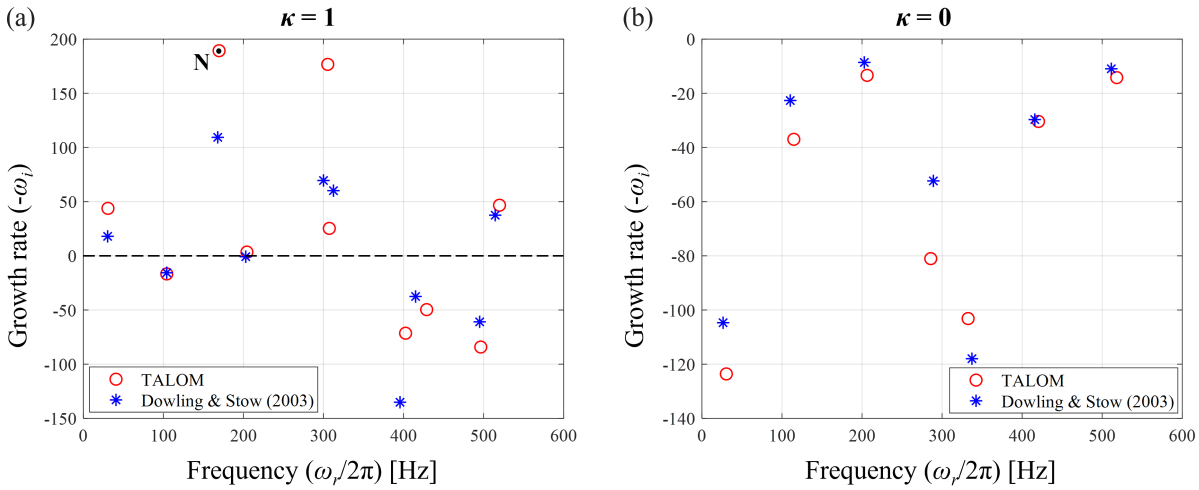

Figure 2: Comparison of eigenvalue spectrum with results by Dowling and Stow [8], with (a) and without (b) unsteady heat release at the flame. The mode of largest growth rate is marked as N; its frequency is 169.5 Hz

3. ADJOINT EQUATIONS

There are two ways to perform the adjoint analysis: continuous adjoint (CA) and discrete adjoint (DA). The difference between these two approaches is the order in which the adjoint equations are derived and discretized. In this paper, we only show the derivation of the CA approach, i.e. the adjoint equations are first derived and their discretization is carried out afterwards.

To build the adjoint eigenvalue problem for the model, we first define the following inner products:
(1) For functions $a(x)$ and $b(x)$:

$$\langle a(x), b(x)\rangle = \int_0^{l_1^-} a(x)^* b(x)\mathrm{d}x + \int_{l_1^+}^{l_2^-} a(x)^* b(x)\mathrm{d}x + \int_{l_2^+}^{l_3} a(x)^* b(x)\mathrm{d}x. \tag{10}$$

(2) For non-spatial functions a and b:

$$\{a, b\} = a^* b. \tag{11}$$

The symbol * denotes the complex conjugate. A set of adjoint variables (Lagrange multipliers) is introduced by defining a Lagrangian functional $\mathcal{L}$ which contains the constraints. For our problem, this functional is defined as:

$$\begin{aligned}\mathcal{L} \equiv \omega &- \left\langle \hat{\rho}^\dagger, E_1 \right\rangle - \left\langle \hat{u}^\dagger, E_2 \right\rangle - \left\langle \hat{p}^\dagger, E_3 \right\rangle - \left\{ \hat{f}_1^\dagger, J_1 \right\} - \left\{ \hat{f}_2^\dagger, J_2 \right\} - \left\{ \hat{f}_3^\dagger, J_3 \right\} - \left\{ \hat{f}_4^\dagger, J_4 \right\} - \left\{ \hat{f}_5^\dagger, J_5 \right\} - \left\{ \hat{f}_6^\dagger, J_6 \right\} \\ &- \left\langle R^\dagger, B_1 \right\rangle - \left\langle U^\dagger, B_2 \right\rangle - \left\langle P^\dagger, B_3 \right\rangle - \left\{ h_1^\dagger, I_1 \right\} - \left\{ h_2^\dagger, I_2 \right\} - \left\{ h_3^\dagger, I_3 \right\} - \left\{ h_4^\dagger, I_4 \right\} - \left\{ h_5^\dagger, I_5 \right\} - \left\{ h_6^\dagger, I_6 \right\},\end{aligned} \tag{12}$$

where E, J, B, and I represent the perturbation equations, the perturbation jump conditions, the base flow equations, and the base flow jump conditions, respectively. The adjoint variables introduced for the perturbation equations are $\hat{\rho}^\dagger$, $\hat{u}^\dagger$, $\hat{p}^\dagger$; for the unsteady flow jump conditions they are $\hat{f}_i^\dagger$, $i = 1, ...6$; for the base flow governing equations they are $R^\dagger$, $U^\dagger$, $P^\dagger$; for the base flow jump conditions they are $h_i^\dagger$, $i = 1, ...6$.

3.1. Adjoint Perturbation Equations

The unsteady flow governing equations in the frequency domain are:

$$E_1 \equiv i\omega\hat{\rho} + \bar{u}\frac{\mathrm{d}\hat{\rho}}{\mathrm{d}x} + \bar{\rho}\frac{\mathrm{d}\hat{u}}{\mathrm{d}x} = 0, \tag{13a}$$

$$E_2 \equiv i\omega\bar{\rho}\hat{u} + \bar{\rho}\bar{u}\frac{\mathrm{d}\hat{u}}{\mathrm{d}x} + \frac{\mathrm{d}\hat{p}}{\mathrm{d}x} = 0, \tag{13b}$$

$$E_3 \equiv i\omega\hat{p} + \bar{u}\frac{\mathrm{d}\hat{p}}{\mathrm{d}x} + \gamma\bar{p}\frac{\mathrm{d}\hat{u}}{\mathrm{d}x} = 0. \tag{13c}$$

Applying integration by parts in Equation 12 and collecting the derivatives of the Lagrangian with respect to the direct perturbation variables ($\hat{p}$, $\hat{u}$, $\hat{\rho}$) produces the adjoint disturbance equations:

$$i\omega^*\hat{\rho}^\dagger + \bar{u}\frac{\mathrm{d}\hat{\rho}^\dagger}{\mathrm{d}x} = 0, \tag{14a}$$

$$i\omega^*\bar{\rho}\hat{u}^\dagger + \bar{\rho}\bar{u}\frac{\mathrm{d}\hat{u}^\dagger}{\mathrm{d}x} + \bar{\rho}\frac{\mathrm{d}\hat{\rho}^\dagger}{\mathrm{d}x} + \gamma\bar{p}\frac{\mathrm{d}\hat{p}^\dagger}{\mathrm{d}x} = 0, \tag{14b}$$

$$i\omega^*\hat{p}^\dagger + \bar{u}\frac{\mathrm{d}\hat{p}^\dagger}{\mathrm{d}x} + \frac{\mathrm{d}\hat{u}^\dagger}{\mathrm{d}x} = 0. \tag{14c}$$

Organizing the boundary terms generated from integration by parts, we obtain the boundary conditions (Eq. 15) and the jump conditions (Eq. 16) of the adjoint system:

$$\hat{u}_1^\dagger(0) = 0, \quad \hat{\rho}_3^\dagger(l_3) = 0, \quad \bar{u}_3\hat{u}_3^\dagger(l_3) + \bar{c}_3^2\hat{p}_3^\dagger(l_3) = 0. \tag{15}$$

$$\bar{u}_1\bar{\rho}_1[a_1\hat{\rho}_2^\dagger(l_1) - a_2\hat{\rho}_1^\dagger(l_1)] = \gamma(a_2\bar{u}_2\bar{p}_2 - a_1\bar{u}_1\bar{p}_1)\hat{p}_2^\dagger(l_1), \tag{16a}$$

$$a_1\bar{\rho}_1[\frac{1}{a_2}\hat{\rho}_2^\dagger(l_1) - \frac{1}{a_1}\hat{\rho}_1^\dagger(l_1)] + \bar{u}_1[\bar{\rho}_2\hat{u}_2^\dagger(l_1) - \bar{\rho}_1\hat{u}_1^\dagger(l_1)] + a_1\bar{\rho}_1[\frac{1}{a_2}\bar{c}_2^2\hat{p}_2^\dagger(l_1) - \frac{1}{a_1}\bar{c}_1^2\hat{p}_1^\dagger(l_1)] = 0, \tag{16b}$$

$$\frac{\bar{p}_2 - \rho_2\bar{c}_1^2}{1-\gamma}\hat{u}_2^\dagger(l_1) - \bar{p}_1\hat{u}_1^\dagger(l_1) + \bar{u}_2\bar{p}_2\hat{p}_2^\dagger(l_1) - \bar{u}_1\bar{p}_1\hat{p}_1^\dagger(l_1) = 0, \tag{16c}$$

$$a_2[\frac{1}{a_3}\hat{\rho}_3^\dagger(l_2) - \frac{1}{a_2}\hat{\rho}_2^\dagger(l_2)] = \frac{a_2}{a_3}(\bar{u}_3 - \bar{u}_2)\hat{u}_3^\dagger(l_2) + [\frac{a_2}{2a_3}(\bar{u}_3 - \bar{u}_2)^2 - \frac{\kappa\bar{Q}}{\bar{u}_2\bar{\rho}_2}e^{i\omega^*\tau}](1-\gamma)\hat{p}_3^\dagger(l_2), \tag{16d}$$

$$\begin{aligned} &a_3\hat{\rho}_2^\dagger(l_2) - a_2\hat{\rho}_3^\dagger(l_2) + a_3\bar{u}_2\hat{u}_2^\dagger(l_2) + a_2\bar{u}_3\hat{u}_3^\dagger(l_2) - 2a_2\bar{u}_2\hat{u}_3^\dagger(l_2) + a_3\bar{c}_2^2\hat{p}_2^\dagger(l_2) - a_2\bar{c}_2^2\hat{p}_3^\dagger(l_2) \\ &\qquad = (\gamma-1)\hat{p}_3^\dagger(l_2)[a_2(\frac{1}{2}\bar{u}_3^2 - 2\bar{u}_2\bar{u}_3 + \frac{3}{2}\bar{u}_2^2) - a_3\frac{\kappa\bar{Q}}{\bar{\rho}_2\bar{u}_2}e^{i\omega^*\tau}], \end{aligned} \tag{16e}$$

$$\hat{u}_3^\dagger(l_2) - \hat{u}_2^\dagger(l_2) + [\frac{a_2}{a_3}\gamma\bar{u}_2 + (1-\gamma)\bar{u}_3]\hat{p}_3^\dagger(l_2) - \bar{u}_2\hat{p}_2^\dagger(l_2) = 0. \tag{16f}$$

The jump conditions for $\hat{f}_i^\dagger$ are reported in the Appendix. Using the adjoint jump and boundary conditions, the adjoint eigen-problem is again solved by the inverse iteration algorithm. The spectrum of adjoint eigenvalues satisfies the bi-orthogonality condition, i.e., it is the complex conjugate of the direct spectrum [10]. The eigenvector contains the amplitudes of adjoint acoustic waves ($A_+^\dagger$, $A_-^\dagger$) and adjoint entropy waves ($A_e^\dagger$); they are used to reconstruct the shapes of the adjoint modes as:

$$\hat{p}^\dagger = A_+^\dagger e^{ik_+^\dagger x} + A_-^\dagger e^{ik_-^\dagger x} + A_e^\dagger e^{ik_0^\dagger x}, \quad \hat{\rho}^\dagger = -\bar{c}^2 A_e^\dagger e^{ik_0^\dagger x}, \quad \hat{u}^\dagger = -\frac{k_+^\dagger\bar{c}^2}{\alpha_+^\dagger}A_+^\dagger e^{ik_+^\dagger x} - \frac{k_-^\dagger\bar{c}^2}{\alpha_-^\dagger}A_-^\dagger e^{ik_-^\dagger x}, \tag{17}$$

together with the relations:

$$k_\pm^\dagger = \frac{\bar{M}\omega^* \mp |\omega^*|}{\bar{c}(1-\bar{M}^2)}, \quad k_0^\dagger = -\frac{\omega^*}{\bar{u}}, \quad \alpha_\pm^\dagger = \omega^* + \bar{u}k_\pm^\dagger. \tag{18}$$

The derivative of the Lagrangian functional with respect to the eigenvalue provides the normalization condition (Eq. 19), which is used to normalize the adjoint variables after reconstruction:

$$\left\langle\hat{\rho}^\dagger, \hat{\rho}\right\rangle + \left\langle\hat{u}^\dagger, \bar{\rho}\hat{u}\right\rangle + \left\langle\hat{p}^\dagger, \hat{p}\right\rangle + \left\{\hat{f}_6^\dagger, -a_3\kappa\tau\bar{Q}(\frac{\hat{u}_2(l_2)}{\bar{u}_2} + \frac{\hat{\rho}_2(l_2)}{\bar{\rho}_2})e^{-i\omega\tau}\right\} = 1. \tag{19}$$

The shapes of the state variables of the direct system and of the the adjoint variables for the predominant mode at $f = 169.5$ Hz are shown in Fig. 3. The amplitude of the adjoint mode shapes provides the receptivity of the system to a forcing term in the corresponding balance equation. Larger amplitudes indicate that the system is more easily controllable.

3.2. Adjoint Base Flow Equations

In this section, we consider the base flow variables as the superposition of the base flow solution plus an infinitesimal generic disturbance, i.e. $\bar{\rho} = \bar{\rho}_0 + \delta\bar{\rho}$, $\bar{u} = \bar{u}_0 + \delta\bar{u}$, and $\bar{p} = \bar{p}_0 + \delta\bar{p}$. For simplicity, from now on, we omit the subscript "0" from the base flow variables. Before applying the Lagrangian functional, the governing equations and jump conditions must be first linearized around the base flow parameters. The linearized base flow governing equations are:

$$B_1 \equiv \delta\bar{\rho}\frac{\mathrm{d}\bar{u}}{\mathrm{d}x} + \bar{\rho}\frac{\mathrm{d}\delta\bar{u}}{\mathrm{d}x} + \bar{u}\frac{\mathrm{d}\delta\bar{\rho}}{\mathrm{d}x} + \delta\bar{u}\frac{\mathrm{d}\bar{\rho}}{\mathrm{d}x} = 0, \tag{20a}$$

$$B_2 \equiv \delta\bar{\rho}\bar{u}\frac{\mathrm{d}\bar{u}}{\mathrm{d}x} + \bar{\rho}\delta\bar{u}\frac{\mathrm{d}\bar{u}}{\mathrm{d}x} + \bar{\rho}\bar{u}\frac{\mathrm{d}\delta\bar{u}}{\mathrm{d}x} + \frac{\mathrm{d}\delta\bar{p}}{\mathrm{d}x} = 0, \tag{20b}$$

$$B_3 \equiv \delta\bar{u}\frac{\mathrm{d}\bar{p}}{\mathrm{d}x} + \bar{u}\frac{\mathrm{d}\delta\bar{p}}{\mathrm{d}x} + \gamma\delta\bar{p}\frac{\mathrm{d}\bar{u}}{\mathrm{d}x} + \gamma\bar{p}\frac{\mathrm{d}\delta\bar{u}}{\mathrm{d}x} = 0. \tag{20c}$$

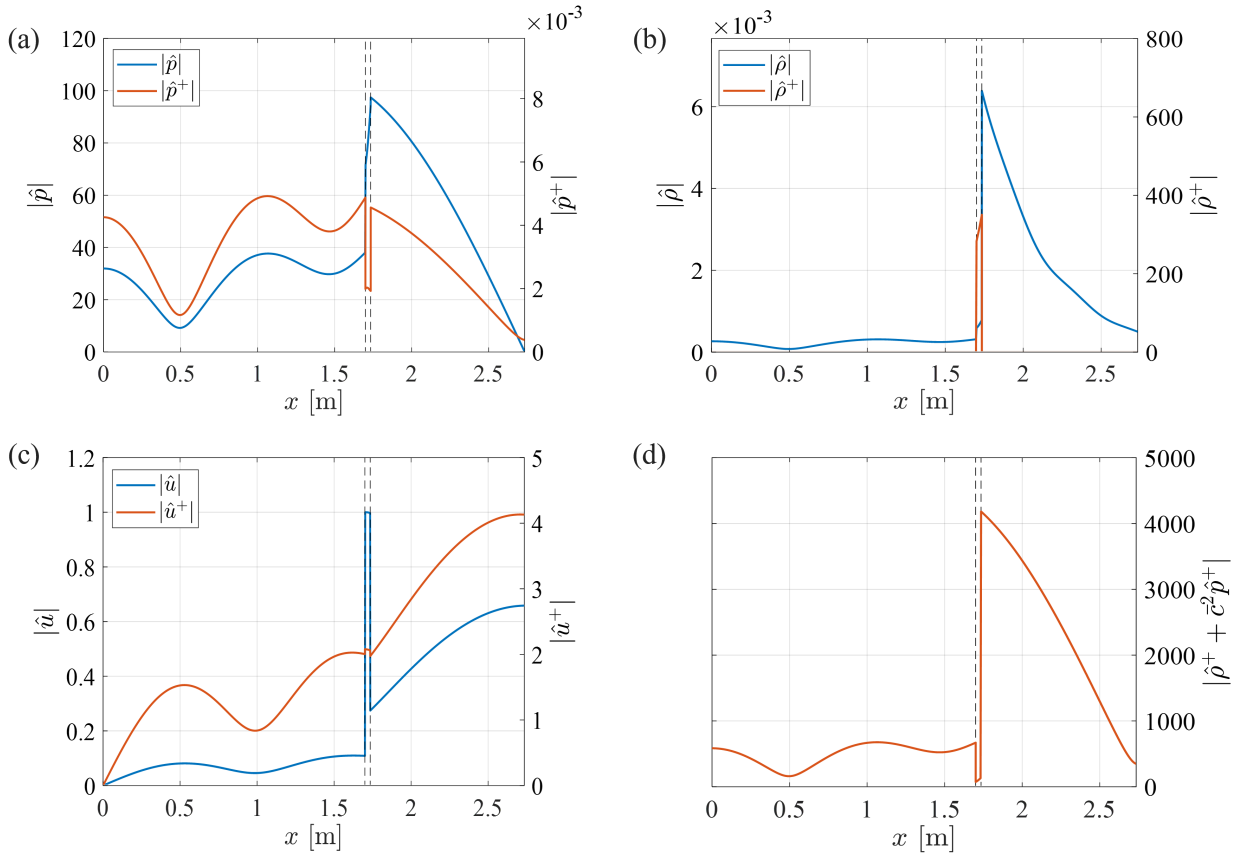

Figure 3: (a)-(c) Mode shapes of direct and adjoint variables for the resonant mode with $f = 169.5$ Hz. The direct perturbations are normalized by the maximum $\hat{u}$ component. The adjoint variables are normalized using Eq. (19). $|\hat{p}^\dagger|$ and $|\hat{u}^\dagger|$ represents the amplitudes of the receptivity of energy and momentum equation, respectively. (d) Amplitude of the receptivity of the continuity equation.

Applying the inner products and integration by parts, the derivatives of the Lagrangian functional with respect to the direct base flow modifications ($\delta\bar{\rho}$, $\delta\bar{u}$, $\delta\bar{p}$), produce the adjoint base flow equations:

$$\bar{u}\frac{\mathrm{d}R^\dagger}{\mathrm{d}x} = \hat{u}^\dagger(i\omega^*)\hat{u}^* + (\hat{\rho}^\dagger + \hat{u}^\dagger\hat{u}^*)\frac{\mathrm{d}\hat{u}^*}{\mathrm{d}x} \tag{21a}$$

$$\bar{\rho}\frac{\mathrm{d}R^\dagger}{\mathrm{d}x} + \bar{\rho}\bar{u}\frac{\mathrm{d}U^\dagger}{\mathrm{d}x} + \gamma\bar{p}\frac{\mathrm{d}P^\dagger}{\mathrm{d}x} = \hat{\rho}^\dagger\frac{\mathrm{d}\hat{\rho}^*}{\mathrm{d}x} + \hat{u}^\dagger\bar{\rho}\frac{\mathrm{d}\hat{u}^*}{\mathrm{d}x} + \hat{p}^\dagger\frac{\mathrm{d}\hat{p}^*}{\mathrm{d}x} \tag{21b}$$

$$\frac{\mathrm{d}U^\dagger}{\mathrm{d}x} + \bar{u}\frac{\mathrm{d}P^\dagger}{\mathrm{d}x} = \gamma\hat{p}^\dagger\frac{\mathrm{d}\hat{u}^*}{\mathrm{d}x} \tag{21c}$$

By a similar procedure it is easy to recover the jump conditions of the adjoint base flow:

$$\left[\frac{\bar{u}_2a_2}{2\bar{u}_1a_1}(\bar{u}_1^2 - \bar{u}_2^2) + \frac{\bar{c}_1^2}{\gamma-1}\left(\frac{\bar{u}_2a_2}{\bar{u}_1a_1} - \frac{\bar{\rho}_1}{\bar{\rho}_2}\right)\right]U_1^\dagger(l_1) + \frac{a_2}{a_1}\bar{c}_1^2\left(\frac{\bar{\rho}_1}{\bar{\rho}_2}\bar{u}_1 - \bar{u}_2\right)P_1^\dagger(l_1) + \frac{a_2}{a_1}\bar{u}_2R_1^\dagger(l_1) = \bar{u}_2R_2^\dagger(l_1), \tag{22a}$$

$$\frac{a_2}{a_1}\left[\frac{2(\bar{c}_2^2 - \bar{c}_1^2) + (\gamma-1)(3\bar{u}_2^2 - \bar{u}_1^2)}{2(\gamma-1)\bar{u}_1}U_1^\dagger(l_1) + \bar{c}_1^2P_1^\dagger(l_1) + R_1^\dagger(l_1)\right] = \bar{u}_2U_2^\dagger(l_1) + \bar{c}_2^2P_2^\dagger(l_1) + R_2^\dagger(l_1), \tag{22b}$$

$$\left(\gamma\frac{\bar{u}_2a_2}{\bar{u}_1a_1} - \frac{\bar{p}_1}{\bar{p}_2}\right)\frac{1}{\gamma-1}U_1^\dagger(l_1) + \frac{\bar{p}_1}{\bar{p}_2}\bar{u}_1P_1^\dagger(l_1) = U_2^\dagger(l_1) + \bar{u}_2P_2^\dagger(l_1), \tag{22c}$$

$$\frac{2a_3\bar{c}_2^2(\bar{u}_3 - \bar{u}_2) + (1-\gamma)\bar{u}_2a_3(\bar{u}_3 - \bar{u}_2)^2}{2a_3(\bar{c}_2^2 - \bar{u}_2^2) + 2\gamma\bar{u}_2^2(a_3 - a_2)}[U_2^\dagger(l_2) + \bar{u}_2P_2^\dagger(l_2)] + \frac{a_3}{a_2}R_2^\dagger(l_2) = R_3^\dagger(l_2), \tag{22d}$$

$$\frac{2a_3(2\bar{u}_3\bar{c}_2^2-\bar{u}_2\bar{c}_3^2-\bar{u}_2\bar{c}_2^2)+(1-\gamma)a_3\bar{u}_2(\bar{u}_3-\bar{u}_2)(3\bar{u}_3-\bar{u}_2)}{2a_3(\bar{c}_2^2-\bar{u}_2^2)+2\gamma\bar{u}_2^2(a_3-a_2)}[U_2^\dagger(l_2)+\bar{u}_2P_2^\dagger(l_2)]+\frac{a_3}{a_2}R_2^\dagger(l_2) = \bar{u}_3U_3^\dagger(l_2)+\bar{c}_3^2P_3^\dagger(l_2)+R_3^\dagger(l_2), \tag{22e}$$

$$\frac{a_3(\bar{c}_2^2-\bar{u}_2^2)+\gamma a_3\bar{u}_2(\bar{u}_2-\bar{u}_3)}{a_3(\bar{c}_2^2-\bar{u}_2^2)+\gamma\bar{u}_2^2(a_3-a_2)}[U_2^\dagger(l_2)+\bar{u}_2P_2^\dagger(l_2)] = U_3^\dagger(l_2)+\bar{u}_3P_3^\dagger(l_2), \tag{22f}$$

and the boundary conditions:

$$U_1^\dagger+P_1^\dagger\bar{u}_1=0, \tag{23a}$$

$$U_3^\dagger+P_3^\dagger\bar{u}_3=0, \tag{23b}$$

$$R_1^\dagger+\bar{u}_1U_1^\dagger+\bar{c}_1^2P_1^\dagger=0, \tag{23c}$$

$$R_3^\dagger+\bar{u}_3U_3^\dagger+\bar{c}_3^2P_3^\dagger=0. \tag{23d}$$

The adjoint variables of the base flow jump conditions ($h_i^\dagger$) are shown in the Appendix. Using the same routine for solving the mean flow, the adjoint base flow variables, $U^\dagger$, $R^\dagger$, and $P^\dagger$ can be solved.

4. SENSITIVITY ANALYSIS

We use $\hat{\mathbf{e}}^\dagger$ to denote the vector of adjoint perturbation variables ($\hat{\rho}^\dagger$, $\hat{u}^\dagger$, $\hat{p}^\dagger$), and use $\mathbf{b}^\dagger$ to denote the vector of adjoint base flow variables ($R^\dagger$, $U^\dagger$, $P^\dagger$). The Lagrangian functional can be written in compact form:

$$\mathcal{L}=\omega-<\hat{\mathbf{e}}^\dagger,E>-\{\hat{f}^\dagger,J\}-<\mathbf{b}^\dagger,B>-\{h^\dagger,I\}. \tag{24}$$

By setting the derivatives of the Lagrangian functional $\mathcal{L}$ with respect to the generic parameter s to zero, the derivative of the eigenvalue with respect to different control parameters of interest can be calculated. It is thus found:

$$\frac{\partial\omega}{\partial s}=\frac{\partial}{\partial s}<\hat{\mathbf{e}}^\dagger,E>+\frac{\partial}{\partial s}\{\hat{f}^\dagger,J\}+\frac{\partial}{\partial s}<\mathbf{b}^\dagger,B>+\frac{\partial}{\partial s}\{h^\dagger,I\}. \tag{25}$$

Next, the structural sensitivity and the base-state sensitivity of the system are evaluated.

4.1. Structural Sensitivity Analysis

In this section we evaluate how the general feedback mechanisms proportional to the state variables applied at position $x = x_0$ will influence the linear stability of the system. An important assumption here is that the feedback mechanisms do not alter the base flow. The feedback mechanisms generating mass addition, momentum addition, and energy addition to the system are denoted as $\mathcal{M}_{\rho,u,p}$, $\mathcal{F}_{\rho,u,p}$, $\mathcal{Q}_{\rho,u,p}$, where the subscripts ρ, u, and p denote a feedback forcing proportional, respectively, to the perturbation state variable $\hat{\rho}$, $\hat{u}$, and $\hat{p}$. In total we have nine different structural perturbations. Any general feedback mechanism can be seen as the linear combination of these nine structural perturbations. The resulting eigenvalue drift is the sum of the eigenvalue drift caused by each individual structural perturbation. They are thus examined separately. For instance, the momentum addition to the system proportional to the pressure perturbation located at $x = x_0$ takes the form:

$$i\omega\bar{\rho}\hat{u}+\bar{\rho}\bar{u}\frac{\mathrm{d}\hat{u}}{\mathrm{d}x}+\frac{\mathrm{d}\hat{p}}{\mathrm{d}x}=\mathcal{F}_p\,\hat{p}\,\delta(x-x_0), \tag{26}$$

where $\delta(x - x_0)$ is the Dirac delta function.

For the continuity equation (E_1) the receptivity to forcing terms is $\hat{\rho}^\dagger + \bar{c}^2\hat{p}^\dagger$; for the momentum equation (E_2) it is $\hat{u}^\dagger$; for the energy equation (E_3) it is $\hat{p}^\dagger$. The structural sensitivity is calculated as

the inner product of receptivity and direct functions. For the case in Eq. (26), the sensitivity of the eigenvalue ω with respect to the feedback mechanism $\mathcal{F}_p$ is:

$$\frac{\delta\omega}{\delta\mathcal{F}_p} = \hat{u}^{\dagger *}(x_0)\hat{p}(x_0). \tag{27}$$

In the same way, the sensitivity functions to other feedback mechanisms can be obtained. The real part of the function is the sensitivity of the angular frequency and the negative imaginary part is the sensitivity of the growth rate. The growth rate shift can affect the stability of the system; the structural sensitivity of the growth rate to the nine feedback mechanisms are shown in Fig. 4.

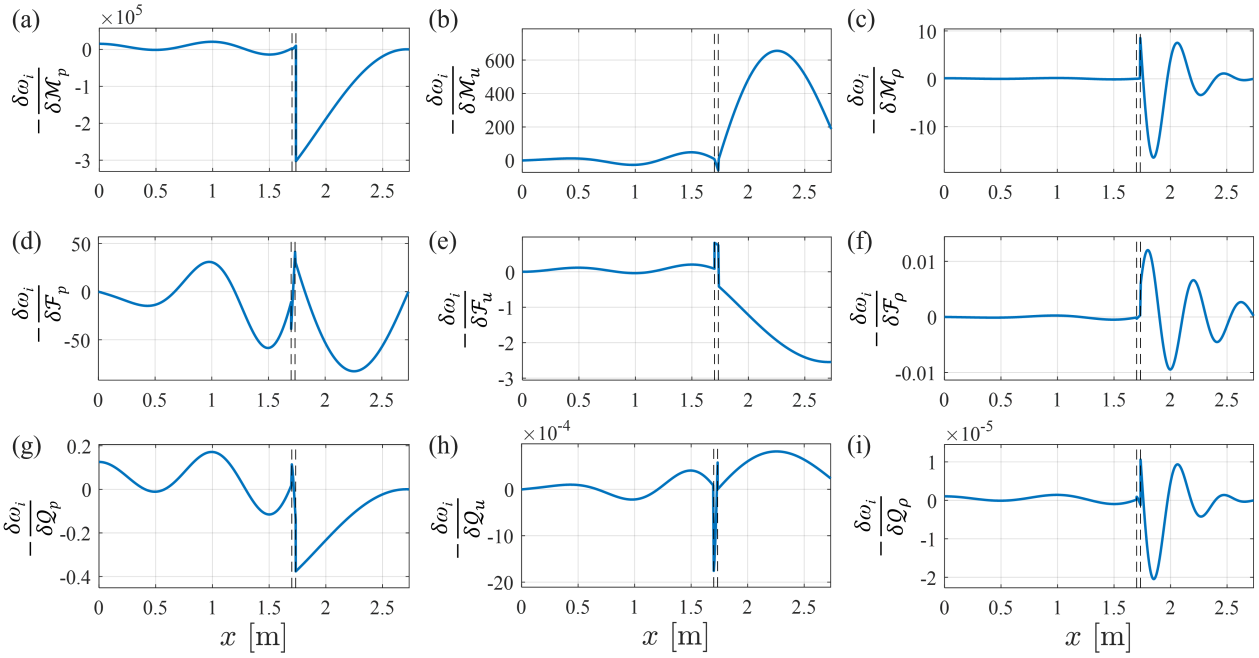

Figure 4: Sensitivity of the growth rate ($-\omega_i$) to generic feedback mechanism proportional to the perturbations.

The positive sensitivity of the growth rate indicates a destabilization effect. For our system, generally, all feedback mechanisms introduced in the plenum section have limited effects on the system's stability. The most stabilizing mechanism is identified as $\mathcal{M}_p$ located downstream of the flame position. Adding mass in proportion to the pressure perturbations can be generated by a Helmholtz resonator. Such mechanism placed in the combustion chamber section will stabilize the system. The closer the Helmholtz resonator is located to the flame region, the more effective is the stabilization mechanism. For the feedback mechanism $\mathcal{M}_u$ the effect is mostly destabilizing.

The stabilizing momentum addition mechanism is identified for $\mathcal{F}_p$ placed within the section of $x = [0, 0.7] \cap [1.2, l_1^-] \cap [1.8, l_3]$. The most efficient position is at $x = 2.3$. For $\mathcal{F}_u$ acting in the premixer destabilization occurs while an action in the combustion chamber will stabilize the system. The most influential stabilizing effect is at the outlet.

For energy addition mechanisms, the effects on growth rate is limited when compared to the other mechanisms. In particular, the effects of $\mathcal{Q}_u$ and $\mathcal{Q}_\rho$ on the eigenvalue drift are negligible if they act on the system with other feedback mechanisms. For $\mathcal{Q}_p$, the sensitivity behavior is similar to that of $\mathcal{M}_p$, i.e. $\mathcal{Q}_p$ acting in the combustion chamber will stabilize the system.

4.2. Base-state Sensitivity Analysis

In this section we evaluate the eigenvalue shift due to arbitrary modifications in the base flow. The derivatives of $\mathcal{L}$ to generic base flow variations ($\delta\bar{u}$, $\delta\bar{\rho}$, $\delta\bar{p}$) give the adjoint base flow equations.

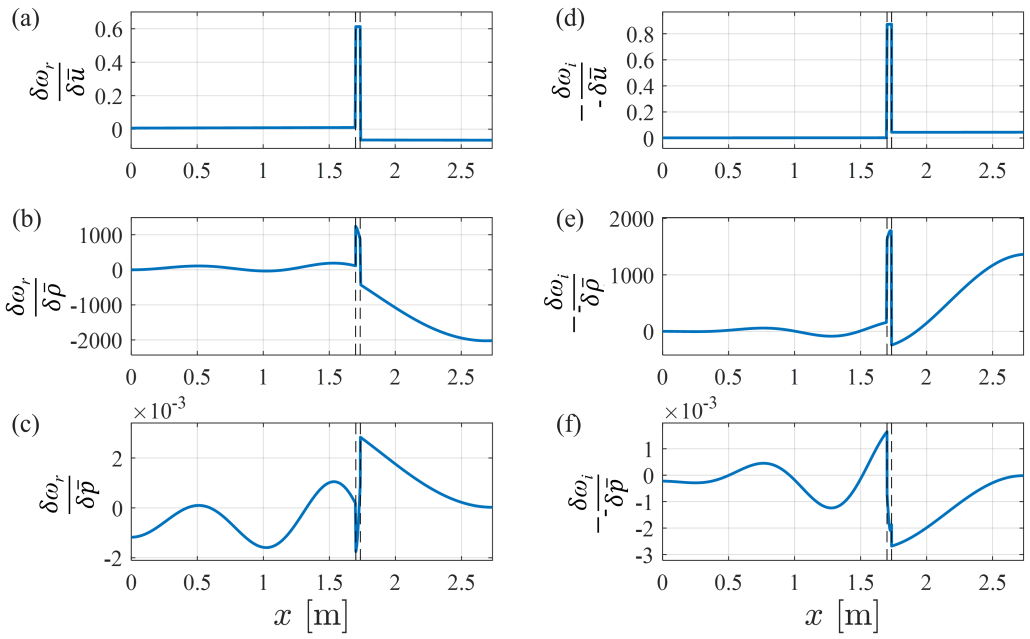

Figure 5: Sensitivity of the angular frequency (ω_r) and of the growth rate ($-\omega_i$) to base flow modifications $\delta\bar{u}$, $\delta\bar{\rho}$, and $\delta\bar{p}$.

Since the adjoint variables are constant in each duct, the sensitivity of eigenvalues to generic base flow modifications ($\delta\bar{u}$, $\delta\bar{\rho}$, $\delta\bar{p}$) can be obtained explicitly from the RHS of Eq. (21), i.e.:

$$\frac{\partial\omega}{\partial\bar{\rho}} = \hat{u}^\dagger i\omega^*\hat{u}^* + (\hat{\rho}^\dagger + \hat{u}^\dagger\hat{u}^*)\frac{\mathrm{d}\hat{u}^*}{\mathrm{d}x}, \tag{28a}$$

$$\frac{\partial\omega}{\partial\bar{u}} = \hat{\rho}^\dagger\frac{\mathrm{d}\hat{\rho}^*}{\mathrm{d}x} + \hat{u}^\dagger\bar{\rho}\frac{\mathrm{d}\hat{u}^*}{\mathrm{d}x} + \hat{p}^\dagger\frac{\mathrm{d}\hat{p}^*}{\mathrm{d}x}, \tag{28b}$$

$$\frac{\partial\omega}{\partial\bar{p}} = \gamma\hat{p}^\dagger\frac{\mathrm{d}\hat{u}^*}{\mathrm{d}x}. \tag{28c}$$

Fig. 5 shows the sensitivity of angular frequency and growth rate of the leading resonant mode N to base flow modifications. It indicates how a generic base flow property increase would change the stability of the system. The most destabilizing effect is found by varying the density at the premixer section. In the combustion chamber, downstream of flame region, there is a slightly stabilizing effect due to density increase up to $x = 1.9$, after which the destabilizing effect grows and peaks near the outlet. For variations in base flow velocity, the most sensitive region for triggering an unstable mode lies within the premixer section. The sensitivity of the leading eigenvalue to a pressure increase appears to be small, with a mild stabilizing effect which can occur in the combustion chamber section.

5. CONCLUSIONS

This study aims to apply adjoint sensitivity analysis to a low-order TA model. The adjoint method analyzes changes in the eigenvalues caused by multiple changes in the system.

An approach denominated TALOM is used to solve Dowling and Stow's one-dimensional premixed combustor model. The resonant modes are identified and corresponds qualitatively to those given in [8]; the most unstable eigenmode of the TA system is found to occur at $f = 169.5$ Hz. The adjoint equations are derived by the Lagrange multiplier approach, based on which the structural and base-state sensitivities are calculated. For the structural sensitivity analysis, we evaluate the angular frequency and growth rate shifts due to generic feedback mechanisms. The most stabilizing effect is

caused by adding mass in a quantity proportional to the local pressure perturbation next to the flame sheet. For the base-state sensitivity, the variation in the leading eigenvalue is examined against mild modifications in the base flow. The most effective base flow modification destabilizing the system is a density increase in the premixer section.

In future work the adjoint sensitivity analysis will be extended to three-dimensional, annular TA systems. Based on the sensitivity analysis outlined here, optimal flow control approaches will be devised to eliminate thermo-acoustic instabilities.

ACKNOWLEDGEMENTS

We would like to thank Dr. Ezio Cosatto for several interesting discussions on the subject of thermo-acoustic modelling. This work is part of the Marie Skłodowska-Curie Innovative Training Network *Pollution Know-How and Abatement* (POLKA). We gratefully acknowledge the financial support from the European Union's Horizon 2020 research and innovation programme under the Marie Skłodowska-Curie grant agreement No. 813367.

APPENDIX: ADJOINT VARIABLES FOR JUMP CONDITIONS

The adjoint variables for the unsteady jump conditions are,

$$\hat{f}_1^\dagger = \frac{1}{a_2}[\hat{\rho}_2^\dagger(l_1) + \bar{c}_2^2\hat{p}_2^\dagger(l_1)], \tag{29a}$$

$$\hat{f}_2^\dagger = \frac{1}{\gamma-1}\bar{p}_2\hat{u}_2^\dagger(l_1) - \bar{u}_2\bar{p}_2\hat{p}_2^\dagger(l_1), \tag{29b}$$

$$\hat{f}_3^\dagger = \bar{\rho}_2\hat{u}_2^\dagger(l_1), \tag{29c}$$

$$\hat{f}_4^\dagger = \frac{1}{a_3}[\hat{\rho}_3^\dagger(l_2) - \bar{u}_3\hat{u}_3^\dagger(l_2) + \frac{\gamma-1}{2}\bar{u}_3^2\hat{p}_3^\dagger(l_2)], \tag{29d}$$

$$\hat{f}_5^\dagger = \frac{1}{a_3}[\hat{u}_3^\dagger(l_2) + (1-\gamma)\bar{u}_3\hat{p}_3^\dagger(l_2)], \tag{29e}$$

$$\hat{f}_6^\dagger = \frac{1}{a_3}(\gamma-1)\hat{p}_3^\dagger(l_2). \tag{29f}$$

The adjoint variables for the base flow jump conditions are,

$$h_1^\dagger = \frac{1}{a_1}[(\frac{\bar{u}_1}{2} + \frac{\gamma\bar{p}_1}{(\gamma-1)\bar{u}_1\bar{\rho}_1})U_1^\dagger(l_1) - \frac{\gamma\bar{p}_1}{\bar{\rho}_1}P_1^\dagger(l_1) - R_1^\dagger(l_1)], \tag{30a}$$

$$h_2^\dagger = -\frac{1}{\bar{u}_1 a_1}U_1^\dagger(l_1), \tag{30b}$$

$$h_3^\dagger = \bar{u}_1\bar{p}_1P_1^\dagger(l_1) - \frac{1}{\gamma-1}\bar{p}_1U_1^\dagger(l_1), \tag{30c}$$

$$h_4^\dagger = \frac{\bar{u}_2[2\bar{c}_2^2 + (\gamma-1)\bar{u}_2^2][U_2^\dagger(l_2) + \bar{u}_2P_2^\dagger(l_2)]}{2a_3[\bar{c}_2^2 + (\gamma-1)\bar{u}_2^2] - 2\gamma a_2\bar{u}_2^2} - \frac{1}{a_2}R_2^\dagger(l_2), \tag{30d}$$

$$h_5^\dagger = \frac{\bar{u}_2(\gamma-1)[U_2^\dagger(l_2) + \bar{u}_2P_2^\dagger(l_2)]}{a_3[\bar{c}_2^2 + (\gamma-1)\bar{u}_2^2] - \gamma a_2\bar{u}_2^2}, \tag{30e}$$

$$h_6^\dagger = \frac{[\bar{c}_2^2 + (\gamma-1)\bar{u}_2^2][U_2^\dagger(l_2) + \bar{u}_2P_2^\dagger(l_2)]}{a_3[\bar{c}_2^2 + (\gamma-1)\bar{u}_2^2] - \gamma a_2\bar{u}_2^2}. \tag{30f}$$

REFERENCES

[1] Timothy C. Lieuwen and Vigor Yang. *Combustion instabilities in gas turbine engines: operational experience, fundamental mechanisms, and modeling*. American Institute of Aeronautics and Astronautics, 2005.

[2] Flavio Giannetti and Paolo Luchini. Structural sensitivity of the first instability of the cylinder wake. *Journal of Fluid Mechanics*, 581:167–197, 2007.

[3] Olivier Marquet, Denis Sipp, and Laurent Jacquin. Sensitivity analysis and passive control of cylinder flow. *Journal of Fluid Mechanics*, 615:221–252, 2008.

[4] Stefano Falco and Matthew P. Juniper. Shape optimization of thermoacoustic systems using a two-dimensional adjoint helmholtz solver. *Journal of Engineering for Gas Turbines and Power*, 143(7), 2021.

[5] José G. Aguilar and Matthew P. Juniper. Shape optimization in low-order thermoacoustic networks. In *GPPS Forum*, volume 18, pages 10–12, 2018.

[6] Luca Magri. Adjoint methods as design tools in thermoacoustics. *Applied Mechanics Reviews*, 71(2), 2019.

[7] José G. Aguilar, Luca Magri, and Matthew P. Juniper. Adjoint-based sensitivity analysis of low-order thermoacoustic networks using a wave-based approach. *Journal of Computational Physics*, 341:163–181, 2017.

[8] Ann P. Dowling and Simon R. Stow. Acoustic analysis of gas turbine combustors. *Journal of Propulsion and Power*, 19(5):751–764, 2003.

[9] Boa-Teh Chu and Leslie S. G. Kovásznay. Non-linear interactions in a viscous heat-conducting compressible gas. *Journal of Fluid Mechanics*, 3(5):494–514, 1958.

[10] Matthew P. Juniper. Adjoints and passive control in thermoacoustics. *Combustion*, 6(3):225–246, 2015.